Rotational excitation of the interstellar NH_2 radical by H_2

Nezha Bouhafs, François Lique, Alexandre Faure, Aurore Bacmann, Jun Li, and Hua Guo

Citation: The Journal of Chemical Physics **146**, 064309 (2017); doi: 10.1063/1.4975324
View online: https://doi.org/10.1063/1.4975324
View Table of Contents: http://aip.scitation.org/toc/jcp/146/6
Published by the American Institute of Physics

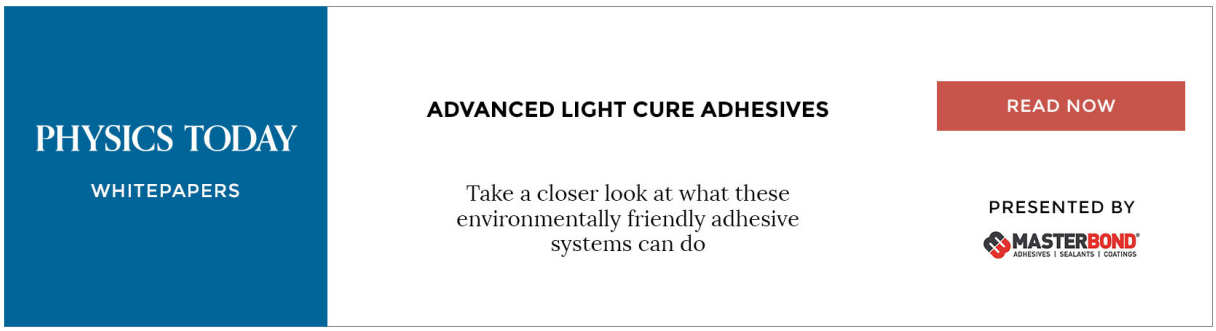

Rotational excitation of the interstellar NH_2 radical by H_2

Nezha Bouhafs,[1] François Lique,[1,a)] Alexandre Faure,[2] Aurore Bacmann,[2] Jun Li,[3,b)] and Hua Guo[3]

[1]*LOMC - UMR 6294, CNRS-Université du Havre, 25 rue Philippe Lebon, BP 1123, 76 063 Le Havre cedex, France*
[2]*UJF-Grenoble 1/CNRS, Institut de Planétologie et d'Astrophysique de Grenoble (IPAG) UMR 5274, Grenoble F-38041, France*
[3]*Department of Chemistry and Chemical Biology, University of New Mexico, Albuquerque, New Mexico 87131, USA*

(Received 4 December 2016; accepted 19 January 2017; published online 13 February 2017)

We present quantum close-coupling calculations for the rotational excitation of the interstellar amidogen radical NH_2 due to collisions with H_2 molecules. The calculations are based on a recent, high-accuracy full-dimensional NH_4 potential energy surface adapted for rigid-rotor scattering calculations. The collisional cross section calculations are performed for all transitions among the first 15 energy levels of both *ortho*- and *para*-NH_2 and for total energies up to 1500 cm^{-1}. Both *para*- and *ortho*-H_2 colliding partners are considered. The cross sections for collision with *para*- and *ortho*-H_2 are found to differ significantly, the magnitude of the *ortho*-H_2 ones being dominant. No strong propensity rules are observed but transitions with $\Delta k_c = 0$ are slightly favored. *Published by AIP Publishing.* [http://dx.doi.org/10.1063/1.4975324]

I. INTRODUCTION

Neutral nitrogen hydrides (NH, NH_2, and NH_3) are highly abundant species in a variety of astrophysical regions. Among them, the NH_2 radical, even if not generally the most abundant one, is of key importance for the chemistry of these media. It was detected for the first time in the interstellar medium (ISM) by van Dishoeck *et al.*[1] who pointed out that this simple hydride is crucial for testing the production pathways of nitrogen-bearing molecules. Indeed, the NH_2 chemistry is directly related to that of the abundant and ubiquitous ammonia, NH_3. In addition, NH_2 exhibit spin symmetry states whose relative abundances are sensitive to the H_2 *ortho-to-para* ratio (OPR) in the gas phase. NH_2 observations[2] may be able to put constraints on the H_2 OPR in dense gas.

The Infrared Space Observatory was later used to observe infrared absorption lines of NH_2[3,4] and recently, the Herschel Space Observatory[5] with the Heterodyne Instrument for the Far-Infrared (HIFI)[6] allowed the observation of several low-lying rotational transitions of NH_2 at a very high spectroscopic resolution.[7] These (absorption) lines were employed to derive NH:NH_2:NH_3 abundance ratios of ~2:1:1 in lukewarm diffuse clouds[8] and ~3:1:20 in the colder envelope of low-mass protostars.[9] Emission lines were also detected more recently in denser and hot ISM regions.[2] In addition, anomalous (non statistical) *ortho*-to-*para* ratios of NH_2 and NH_3 were derived in the diffuse gas.[2,10] These ratios were successfully reproduced by gas-phase models including a rigorous nuclear-spin chemistry,[9,11] suggesting that NH_2, just like NH_3, is mainly formed in the gas-phase via a series of successive hydrogen abstraction reactions $NH_n^+ + H_2$ (n = 0–3) followed by electronic dissociative recombination. A recent study has also emphasized the importance of the H-exchange reaction $NH_2 + H$ in the *ortho-para* conversion of NH_2.[12]

However, the analysis of the NH_2 rotational spectra, especially those in emission, was hampered by the lack of collisional rate coefficients. Without these data, only approximate estimates of the molecular column density are possible assuming local thermodynamic equilibrium (LTE), which is generally not a good approximation. Persson *et al.*[2] estimated collisional rate coefficients assuming quenching rate coefficient of 5×10^{-11} cm^3 s^{-1} and state-specific downward rates for radiatively allowed transitions that scale in proportion to radiative line strengths. Such estimates are very approximate and the accurate determination of the NH_2 abundance would greatly benefit from accurate collisional data. The main collider in the dense ISM is generally molecular hydrogen, H_2.

Scattering studies implying nonlinear polyatomic molecules and H_2 are still sparse. To date, calculations of rate coefficients for the collisional excitation by *para*- and *ortho*-H_2 (hereafter *p*-H_2 and *o*-H_2, respectively) have been performed only for the four interstellar molecules H_2CO,[13] NH_3,[14] CH_3OH,[15] H_2O,[16] and SO_2.[17]

To the best of our knowledge, there are no collisional data available for the NH_2–H_2 system. The only relevant study for astrophysics implying the NH_2 molecules is the measurement of integral cross sections for NH_2–He rotational transitions performed by Dagdigian.[18] However, no rate coefficients were given in this work. NH_2–H collisions were also studied[19] but the NH_2 molecule was in its first excited electronic state that is negligibly populated in astrophysical media.

NH_2 is an asymmetrical rotor with two forms caused by the different relative orientations of the hydrogen nuclear

a)Electronic mail: francois.lique@univ-lehavre.fr
b)Present address: School of Chemistry and Chemical Engineering, Chongqing University, Chongqing 401331, China.

spins. In collision with H_2, the two forms behave like two distinct species: *ortho*-NH_2 and *para*-NH_2 (hereafter denoted as *o*-NH_2 and *p*-NH_2, respectively). In addition, NH_2 has a complex rotational structure resulting from the open-shell character of the NH_2 ground electronic state $^2B_1$. Hence, each rotational level is split by spin-rotation interaction in a fine structure of two sublevels identified by the total angular momentum j_1 with $\vec{j_1} = \vec{N_1} + \vec{S}$ (where N_1 is the rotational angular momentum and S is the electronic spin). Moreover, fine structure levels are further split into three components through hyperfine interactions, due to the coupling between the nitrogen nuclear spin and the total angular momentum j_1. Finally, a second hyperfine structure resulting from the coupling between the nuclear spins of the hydrogen nuclei splits all *o*-NH_2 sublevels into three new sublevels.

The calculation of collisional cross sections taking into account this complex structure is an extremely challenging task. Calculations of collisional data for open-shell molecules in collision with H_2 have been achieved only recently[20] for linear molecules and cannot be easily extended to a polyatomic top. This is why, in the present work, we neglect the fine and hyperfine structure of the NH_2 target and we provide data for transitions between rotational levels. Collisional data including these specific structures may be deduced from the present calculations using decoupling approximations.[21,22]

In this paper, we used a new accurate full-dimensional NH_4 potential energy surface (PES)[23] to compute the cross sections for the collisional excitation of the first 15 rotational levels of both *o*- and *p*-NH_2 by H_2. The paper is organized as follows. The PES and the scattering calculations are presented in Section II. In Section III, we report state-to-state resolved cross sections for the rotational excitation of NH_2 by H_2. Concluding remarks are drawn in Section IV.

II. METHODS

A. Potential energy surface

The NH_2 radical is known to react with H_2 to form NH_3 through an exothermic pathway by a direct hydrogen abstraction mechanism. This reactive channel $NH_2 + H_2 \rightarrow NH_3 + H$ was found to have a barrier of 3340 cm^{-1}.[23] The reaction is thus quite slow with rate coefficients lower than 10^{-15} $cm^3\ s^{-1}$ for temperatures lower than 500 K.[23,24] Under such circumstances, neglecting the reactive pathway in the treatment of the NH_2–H_2 collision should have only a small influence on the description of the inelastic processes,[25,26] as long as low to moderate collision energies are considered. We also note that the hydrogen exchange process is also negligibly small under such conditions.

An accurate rigid-rotor five-dimensional PES was then constructed for the NH_2–H_2 system in its electronic and vibrational ground state, suitable for low-energy inelastic rotational calculations, from the recently computed nine-dimensional global PES of NH_4.[23] This PES was determined at the UCCSD(T)-F12a/aug-cc-pVTZ level of theory and the *ab initio* points were fitted using the permutation-invariant polynomial neutral network (PIP-NN) method[27] with a root mean squared error (RMSE) of 27 cm^{-1}. The RMSE of 27 cm^{-1} is for the full nine-dimensional PES (including the reactive path). The fitting RMSE for the non-reactive NH_2–H_2 region relevant for this work is much smaller, of the order of few cm^{-1}.

In this work, the intermolecular potential is described as a function of five coordinates, namely, the intermolecular distance R from the NH_2 center of mass to the H_2 center of mass, and four relative angles (θ, φ) and (θ', φ') which describe, respectively, the collision direction and the H_2 orientation relative to the NH_2 body-fixed system. The body-fixed Jacobi coordinate system used in our calculations is presented in Fig. 1.

As the original routine from Li and Guo[23] employs internuclear coordinates, the following transformation was employed to determine the Cartesian positions of the two hydrogen atoms (H_a with coordinates x_a, y_a, z_a and H_b with coordinates x_b, y_b, z_b) of the H_2 molecule in the NH_2 body-fixed coordinate system:

$$x_a = R\sin\theta\cos\varphi + r_{H_2}\sin\theta'\cos\varphi'\frac{m_H}{2m_H}, \quad (1)$$

$$y_a = R\sin\theta\sin\varphi + r_{H_2}\sin\theta'\sin\varphi'\frac{m_H}{2m_H}, \quad (2)$$

$$z_a = R\cos\theta + r_{H_2}\cos\theta'\frac{m_H}{2m_H}, \quad (3)$$

$$x_b = R\sin\theta\cos\varphi - r_{H_2}\sin\theta'\cos\varphi'\frac{m_H}{2m_H}, \quad (4)$$

$$y_b = R\sin\theta\sin\varphi - r_{H_2}\sin\theta'\sin\varphi'\frac{m_H}{2m_H}, \quad (5)$$

$$z_b = R\cos\theta - r_{H_2}\cos\theta'\frac{m_H}{2m_H}, \quad (6)$$

where r_{H_2} is the bond length of H_2 fixed at its vibrationally averaged distance $\langle r_{H_2}\rangle_0 = 1.449\ a_0$. The NH_2 molecule, which lies in the (xoz) plane (see Fig. 1), was also kept rigid with an averaged geometry taken from the experimental work of Davies *et al.*:[28] $\langle r_{NH}\rangle_0 = 1.936\ a_0$ and $\langle\widehat{HNH}\rangle_0 = 103.33°$. We note that employing state-averaged geometries is a reliable approximation for including zero-point vibrational effects within a rigid-rotor PES, as discussed in previous studies on H_2O–H_2.[29,30] In addition, it was shown recently for the CO–H_2 system that state-averaged geometries also give scattering results very close to full-dimensional calculations.[31]

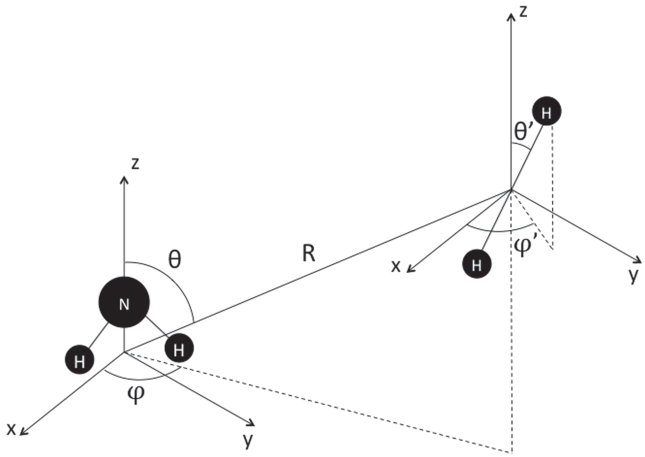

FIG. 1. Jacobi coordinate system of the NH_2–H_2 complex.

Here, the lowest vibrational bending frequency of NH_2 is $\simeq$1500 cm^{-1}.[32] Hence, vibrational excitation is closed at the investigated energies and can be safely neglected in the scattering calculations.

The original fit of Li and Guo[23] was employed to generate interaction energies on a very dense grid of 81 000 geometries in $R, \theta, \varphi, \theta'$, and φ'. An asymptotic potential of 2062.47 cm^{-1} (corresponding to the above monomer averaged geometries) was subtracted from these interaction energies. 27 values in R were selected in the range [3.75–20.00]a_0 and this radial grid was combined with 3000 random angular geometries $\theta, \varphi, \theta', \varphi'$. The PES $V(R, \theta, \varphi, \theta', \varphi')$ was expanded over angular functions for all R-distances using the following expression:[33]

$$V(R,\theta,\varphi,\theta',\varphi') = \sum v_{p_1q_1p_2p}(R) t_{p_1q_1p_2p}(\theta,\varphi,\theta',\varphi'), \quad (7)$$

where

$$t_{p_1q_1p_2p}(\theta,\varphi,\theta',\varphi') = (1+\delta_{q_10})^{-1} \sum \begin{pmatrix} p_1 & p_2 & p \\ r_1 & r_2 & r \end{pmatrix} \times Y_{p_2r_2}(\theta',\varphi') Y_{pr}(\theta,\varphi) \times \left[\delta_{q_1r_1} + (-1)^{p_1+q_1+p_2+p}\delta_{-q_1r_1}\right], \quad (8)$$

where $(3j)$ is a "3-j" symbol, Y_{pq} is a spherical harmonic, δ_{ij} is a Kronecker delta, equal to one if $i = j$ and to zero otherwise, and the sum is over r_1, r_2, r. The indices p_1, p_2, and p refer to the tensor ranks of the angle dependence of the NH_2 orientation, the H_2 orientation, and the collision vector orientation, respectively. In Eq. (8), the index of the C_{2v} symmetry of NH_2 requires that q_1 be even and the homonuclear symmetry of H_2 similarly constrains p_2 to be even. The expansion coefficients $v_{p1q1p2p}(R)$ were obtained through a least-squares fit on the random grid of 3000 orientations at each intermolecular separation. We initially included all anisotropies up to $p_1 = 10$, $p_2 = 6$, and $p = 16$, resulting in 810 basis functions. We then selected only significant terms using a Monte Carlo error estimator (defined in the work of Rist and Faure[34]), resulting in a final set of 146 expansion functions with anisotropies up to $p_1 = 10$, $p_2 = 6$, and $p = 13$. The RMSE was found to be lower than 1 cm^{-1} for $R > 4.75\,a_0$. A cubic spline interpolation of the coefficients $v_{p_1q_1p_2p}(R)$ was finally performed over the whole R range and it was smoothly connected using a switching function to standard extrapolations (exponential and power laws at the short and long-range, respectively) in order to provide continuous radial expansion coefficients for the scattering calculations. Figure 2 shows a sample of expansion coefficients ($v_{p_1q_1p_2p}$) of the NH_2–H_2 PES, as a function of intermolecular distance R.

Two-dimensional plots of the NH_2–H_2 PES are presented in Figs. 3–5.

The global minimum of the 5D fitted PES is located at $\theta = \theta' = 0°$ with a depth of −213.00 cm^{-1} and at an intermolecular distance $R = 6.05\,a_0$. This minimum corresponds to the most stable configuration of the NH_2–H_2 complex so that H_2 is approaching the N atom of the NH_2 molecule along the C_2 axis.

In Fig. 3, we show a contour plot of the interaction energy for fixed $\theta' = \varphi = \varphi' = 0°$. This plot shows the anisotropy of the interaction with respect to the NH_2 rotation.

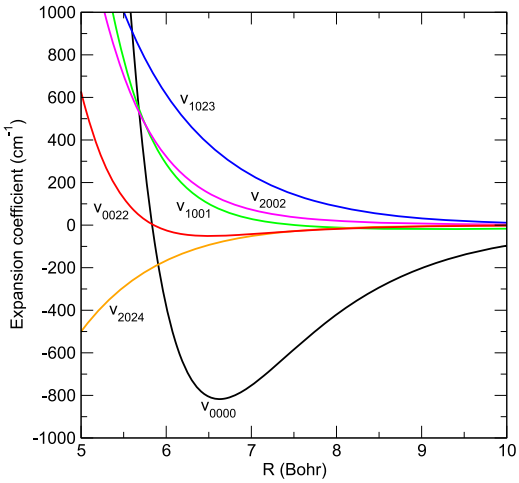

FIG. 2. Sample of expansion coefficients ($v_{p1q1p2p}$) of the NH_2–H_2 PES, as function of intermolecular distance R, for p_1 = 0,1,2 and p_2 = 0,2.

Figure 4 shows the interaction energies for $\varphi = \varphi' = 0°$ and $R = 6.05\,a_0$. We found a relatively strong anisotropy of the PES with respect to the NH_2 and H_2 rotation. It means that the rotational state of H_2 will probably influence the magnitude of the NH_2 excitation cross sections.

A secondary minimum is found at $\theta = 113°$, with an energy deduced from our fit of −122.29 cm^{-1}. It occurs when H_2 is approaching along the direction of the NH bond and H_2 is perpendicular to the NH_2 plane ($\theta' = \varphi' = 90°$). The contour plot is displayed in Fig. 5.

Finally, it is interesting to compare the NH_2–H_2 with the H_2O–H_2 PES of Valiron *et al.*[29] The shape of the two PESs is quite similar. Indeed, Valiron *et al.*[29] reported that the H_2O–H_2 global minimum is at the same configuration than that of NH_2–H_2, the well depth of H_2O–H_2 and NH_2–H_2 PESs being similar (−235.14 cm^{-1} for the H_2O–H_2 complex vs. −213 cm^{-1} for the NH_2–H_2 complex).

Furthermore, for both NH_2–H_2 and H_2O–H_2 PESs, a secondary minimum is found when H_2 is approaching along the direction of the NH (OH) bond with the H_2 molecule perpendicular to the NH_2 (H_2O plane). The H_2O–H_2 secondary minimum found at $\theta = 119°$ and $\theta' = 90°$ with a well depth equal to −199.40 cm^{-1} is, however, deeper than that of NH_2–H_2 (−122.29 cm^{-1}) found at $\theta = 113°$ and $\theta' = 90°$.

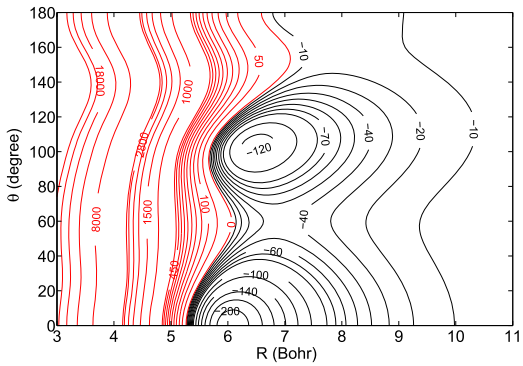

FIG. 3. Contour plot of the 5D PES as function of R, θ for fixed $\theta' = \varphi = \varphi' = 0°$. Energy is in cm^{-1}.

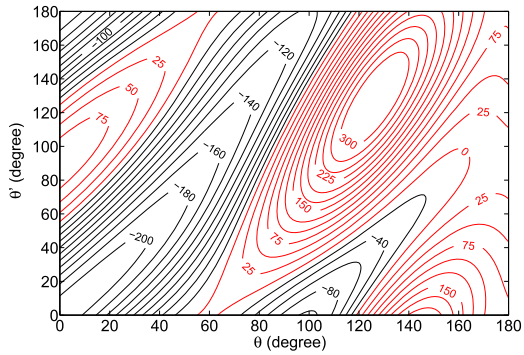

FIG. 4. Contour plot of the 5D PES as function of θ, θ' for fixed $\varphi = \varphi' = 0°$ at an intermolecular separation of $R = 6.05$ a_0. Energy is in cm^{-1}.

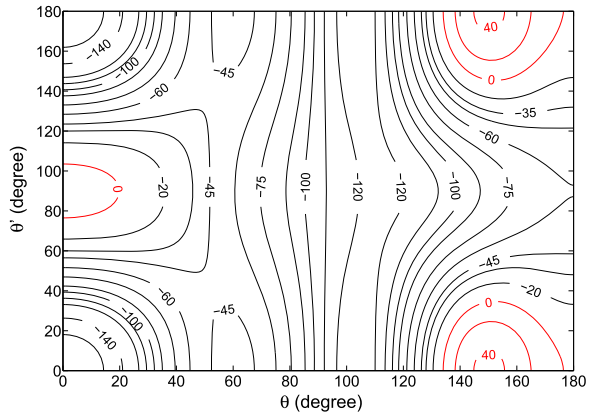

FIG. 5. Contour plot of the 5D PES for fixed $\varphi = 0°$, $\varphi' = 90°$, and $R = 6.61 a_0$ corresponding to the secondary minimum. Energy is in cm^{-1}.

B. Scattering calculations

We used the fitted NH_2–H_2 PES to study the rotational excitation of NH_2 by H_2.

We focus only on the collisional excitation of the rotational states of NH_2, since the computation of fine/hyperfine structure resolved cross sections is a true challenge. The rotational energy levels of NH_2 are labelled by three numbers: the angular momentum N_1 and the pseudo-quantum numbers k_a and k_c which correspond to the projection of N_1 along the axis of the least and greatest moments of inertia, respectively. The *para* states correspond to $k_a + k_c$ odd and the *ortho* states to $k_a + k_c$ even. Extension to the fine/hyperfine structure using approximate treatment will be considered in a future study.

The rotational levels of NH_2 were obtained using the rotational constants from Müller *et al.*[35] Figure 6 shows the rotational energy levels of both *o*- and *p*-NH_2. For the H_2 molecule, the rotational states are denoted by j_2 throughout this paper. The *para* states of H_2 have even rotational states $j_2 = 0, 2, \ldots$ and the *ortho* states have odd rotational states, $j_2 = 1, 3, \ldots$.

As inelastic (nonreactive) collisions cannot interconvert the *ortho*- and *para*-forms, the calculations were done separately for the four spin combinations, namely, *p*-NH_2–*p*-H_2, *p*-NH_2–*o*-H_2, *o*-NH_2–*p*-H_2, and *o*-NH_2–*o*-H_2. NH_2 molecule is treated as a rigid rotor. We used the quantum close-coupling (CC) approach to obtain the inelastic cross sections as described in Phillips *et al.*[36] All scattering calculations have been performed with the version 14 of the MOLSCAT code.[37] The coupled equations were solved using the modified log-derivative airy propagator of Alexander and Manolopoulos.[38] The reduced mass of the system is 1.790 367 amu.

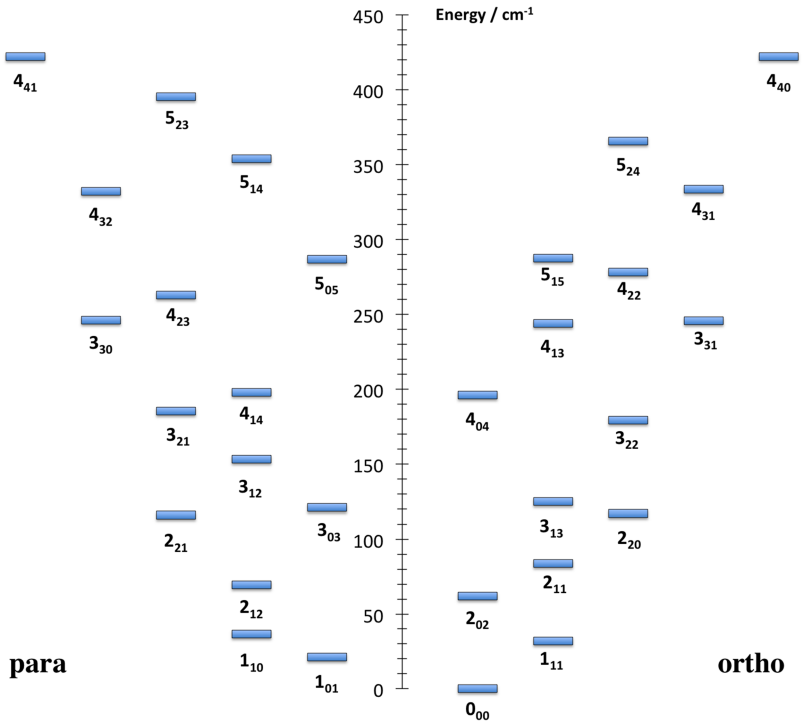

FIG. 6. Diagram of the rotational energy levels of NH_2. The levels are labelled by the $N_{1k_ak_c}$ quantum numbers.

Inelastic cross sections were obtained between levels with a rotational energy $E_{rot} \leq 422\ cm^{-1}$, that is, up to $N_{1k_ak_c} = 4_{40}$ for o-NH_2 and $N_{1k_ak_c} = 4_{41}$ for p-NH_2.

The collisions were studied for the total energy ranging from 32 to 1500 cm^{-1}. The integration parameters were chosen to ensure convergence of the cross sections in this range. We carefully spanned the energy range to guarantee a good description of the resonances. For collision with p-H_2, the energy steps are 0.2 cm^{-1} below 100 cm^{-1}, 0.5 cm^{-1} from 100 to 200 cm^{-1}, 1.0 cm^{-1} from 200 to 500 cm^{-1}, 2.0 cm^{-1} from 500 to 700 cm^{-1}, 5.0 cm^{-1} from 700 to 1000 cm^{-1}, and 20 cm^{-1} from 1000 to 1500 cm^{-1}. For collision with o-H_2, the energy steps are 0.2 cm^{-1} below 300 cm^{-1}, 1.0 cm^{-1} from 200 to 500 cm^{-1}, 2.0 cm^{-1} from 500 to 700 cm^{-1}, 5.0 cm^{-1} from 700 to 1000 cm^{-1}, and 20 cm^{-1} from 1000 to 1500 cm^{-1}. At each collision energy, the total angular momentum J_{tot} was set large enough to converge cross sections, the value of J_{tot} varies from 19 at low energies to 64 for energies larger than 1000 cm^{-1}.

Since a given N_1 rotational number includes a large number of NH_2 sub-rotational energy, rotational levels with internal energies above $E_{max} = 650\ cm^{-1}$ were eliminated for total energies $E_{tot} \leq 200\ cm^{-1}$. This E_{max} parameter was progressively increased up to $E_{max} = 2200\ cm^{-1}$ for $E_{tot} = 1500\ cm^{-1}$. These large values of E_{max} are needed to converge cross sections. A similar effect was previously observed for methyl-formate ($HCOOCH_3$) colliding with helium[39] and for formaldehyde (H_2CO) colliding with H_2.[40]

It was also crucial to optimize the rotational basis of H_2 in order to keep calculations feasible in terms of both central processing unit (CPU) time and memory. Tests of the p-H_2 and o-H_2 basis were performed at different values of total energy. For collisions with p-$H_2(j_2 = 0)$, the inclusion of the $H_2(j_2 = 2)$ level was necessary to obtain cross sections converged to better than 5%, even when these channels were energetically closed. For o-$H_2(j_2 = 1)$, it was found that inclusion of the $H_2(j_2 = 3)$ level in the basis does not have a noticeable influence on the magnitude of the cross sections. Hence, for the determination of rotational excitation cross section of NH_2 in collision with o-H_2, only the $H_2(j_2 = 1)$ basis was retained.

III. RESULTS

Figure 7 shows the collisional energy dependence of the de-excitation integral cross sections of o- and p-NH_2 in collision with o-$H_2(j_2 = 1)$ and p-$H_2(j_2 = 0)$. One can first observe resonances that appear for energies lower than 250 cm^{-1}. These resonances in the de-excitation cross sections are related to the presence of the attractive potential well with a depth of −213 cm^{-1} that allows the H_2 molecule to be temporarily trapped and hence quasi-bound states to be formed before the complex dissociates. The cross sections for collisions with p-$H_2(j_2 = 0)$ seem to display a richer resonance structure than the cross sections for collisions with o-$H_2(j_2 = 1)$ that appear to have a smoother energy dependence. Actually, there are many more, and hence overlapping, resonances for the cross sections for collisions with o-$H_2(j_2 = 1)$ because of a larger number of (quasi-)bound states due to the contribution of an additional coupling term $N_1 + j_2 = j_{12}$ absent in collisions with p-$H_2(j_2 = 0)$. Second, regarding the magnitude of the cross sections, we observe a global decrease of their intensity with increasing ΔN_1. However it is interesting to note that for collisions with p-$H_2(j_2 = 0)$, the magnitude of cross sections with $\Delta N_1 = 2$ can be larger than those with $\Delta N_1 = 1$, while the trend is a rather monotonic decrease for o-$H_2(j_2 = 1)$.

Also, when the collisional energy increases, the magnitude of the cross sections for $\Delta N_1 = 1$ and $\Delta N_1 > 1$ tends to be closer whether for collisions with p- or o-H_2. This behavior is expected and observed for many systems like HNC–H_2,[41] HCl–H_2,[42] and O_2–H_2.[43]

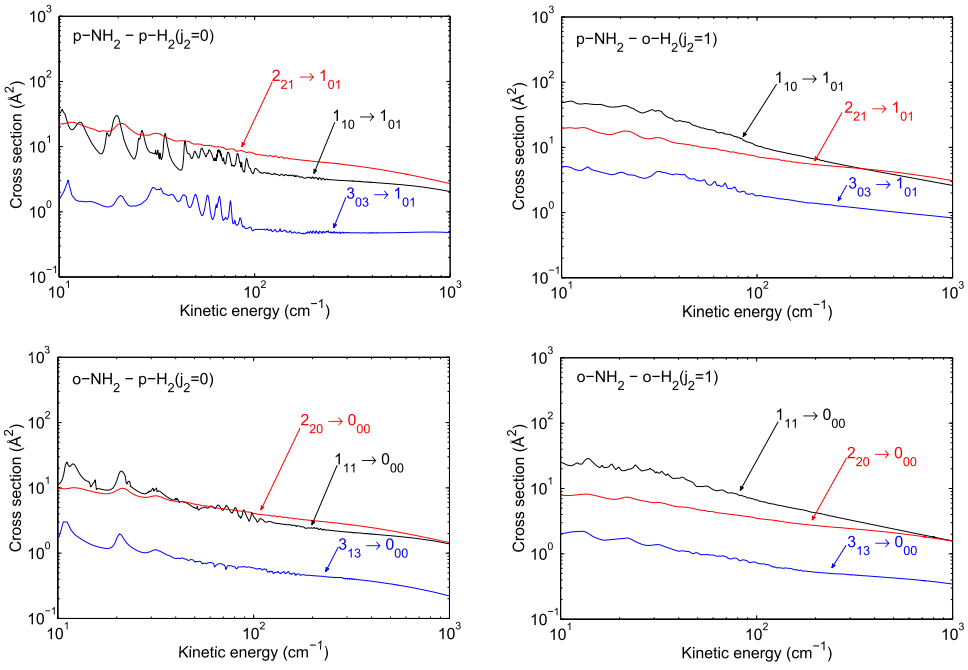

FIG. 7. Rotational de-excitation cross sections of *para*- and *ortho*-NH_2 by *para*- and *ortho*-H_2. For collisions with both p- and o-H_2, j_2 is unchanged.

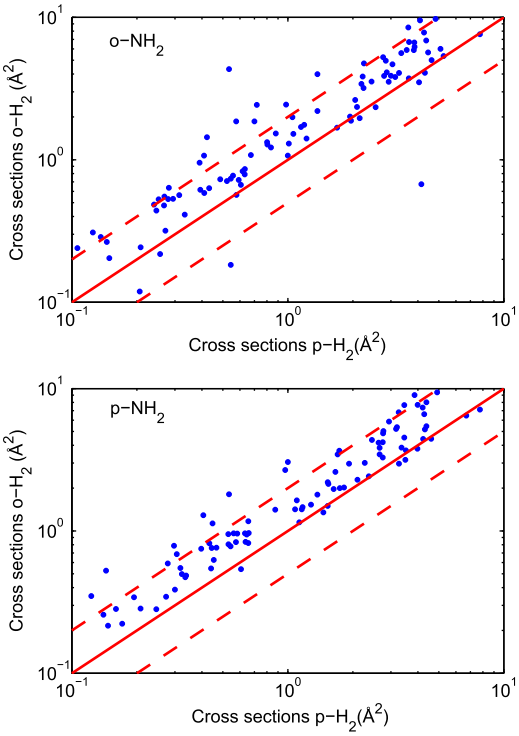

FIG. 8. Comparison between p- and o-H_2 de-excitation cross sections for o-NH_2 (upper panel) and p-NH_2 (lower panel) at a collision energy of 100 cm^{-1}. The horizontal axis represents the collisional cross sections with p-$H_2(j_2 = 0)$ and the vertical axis represents the corresponding collisional cross sections with o-$H_2(j_2 = 1)$. The two dashed lines in each panel delimit the region where the cross sections differ by less than a factor 3.

In order to have an overview of the differences that exist between the excitation cross sections with p- and o-H_2 colliders, we show, in Fig. 8, a comparison between the two sets of cross sections for all the de-excitation transitions from all initial levels up to $N_{1k_ak_c} = 4_{40}$ for o-NH_2 and up to $N_{1k_ak_c} = 4_{41}$ for p-NH_2 at a fixed collision energy of 100 cm^{-1}. The horizontal axis presents the cross sections for collisions with p-$H_2(j_2 = 0)$ whereas the vertical axis presents the cross sections for collisions with o-$H_2(j_2 = 1)$.

Examination of the plots for collisions of o- and p-NH_2 with both o- and p-H_2 shows that the two sets of data agree generally within a factor of 3. The largest cross sections are those for collision with o-H_2, with only a few exceptions. This trend was already observed for several interstellar species like SiS,[44] HCl,[42] SO_2,[45] or H_2O.[46]

This behavior can also be explained by looking at the radial coefficients $\upsilon_{p_1q_1p_2p}$ of the expansion Equation (7), as plotted in Fig. 2. The radial coefficients contributing to cross sections with $j_2 \rightarrow j_2'$ transitions are those with p_2 in the range $j_2 - j_2' < p_2 < j_2 + j_2'$. Then, for collisions with p-$H_2(j_2 = 0)$ only the terms with $p_2 = 0$ contribute whereas for collisions with o-$H_2(j_2 = 1)$ the $p_2 = 0$, 2 terms contribute. The radial coefficients with $p_2 = 2$ are not negligible compared to the one with $p_2 = 0$ explaining why the cross sections for collisions with o-$H_2(j_2 = 1)$ are larger than the ones for collisions with p-$H_2(j_2 = 0)$. The non-negligible contribution of the radial coefficients with $p_2 = 2$ can be explained notably by the dipole-quadrupole interaction that exists for collisions with o-H_2 and that vanishes for collisions with p-H_2.

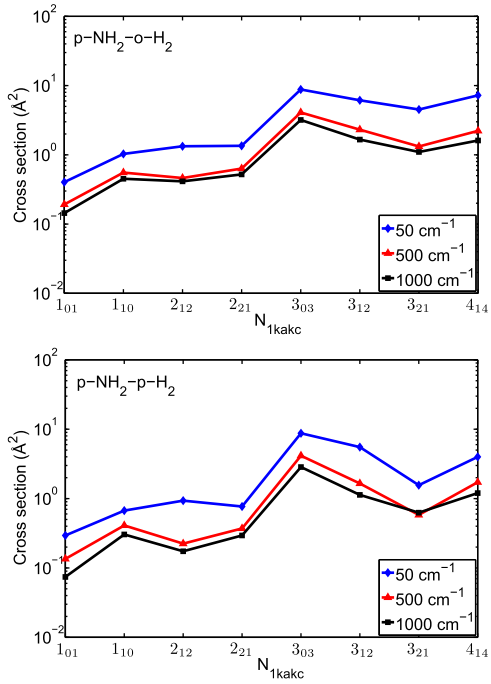

FIG. 9. Propensity rules for transitions out of the initial $N_{1k_ak_c} = 4_{23}$ state of the p-NH_2 molecule in collision with p-$H_2(j_2 = 0)$ (bottom panel) and o-$H_2(j_2 = 1)$ (top panel), for kinetic energies = 50, 100, and 1000 cm^{-1}.

Then, we were interested in the propensity rules in the NH_2–H_2 collisional system. Figures 9 and 10 show, at 3 different collisional energies (50, 500, and 1000 cm^{-1}), the rotational de-excitation cross sections from p-$NH_2(N_{1k_ak_c} = 4_{23})$ and o-$NH_2(N_{1k_ak_c} = 4_{13})$ for both p- and o-H_2 collisions.

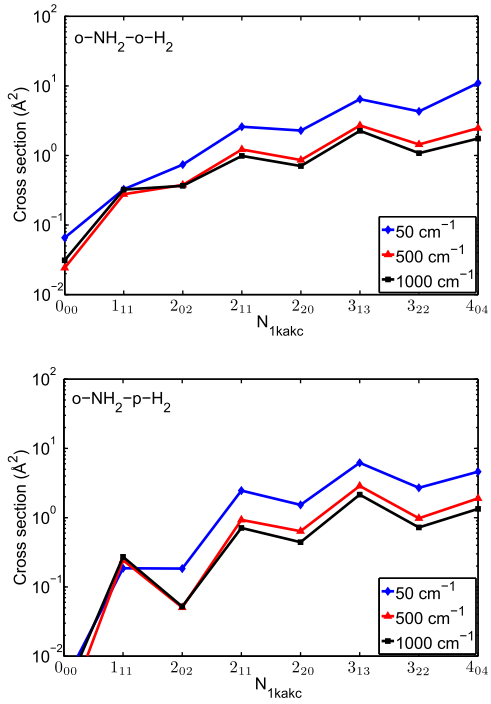

FIG. 10. Propensity rules for transitions out of the initial $N_{1k_ak_c} = 4_{13}$ state of the o-NH_2 molecule in collision with p-$H_2(j_2 = 0)$ (bottom panel) and *ortho*-$H_2(j_2 = 1)$ (top panel), for kinetic energies = 50, 100, and 1000 cm^{-1}.

TABLE I. Comparison of cross sections for transitions out of *o*-$NH_2(N_{1k_ak_c} = 0_{00})$ rotational level induced by collisions with *p*-$H_2(j_2 = 0)$ and He.[18] $E_{col} = 467\ cm^{-1}$.

	Cross sections	
Final level	*o*-NH_2–*p*-H_2	*o*-NH_2–He
1_{11}	(1)[a]	(1)[a]
2_{02}	(1)[a]	(1)[a]
2_{11}	0.01	≤0.05 ± 0.02
3_{13}	0.37	0.07 ± 0.02
4_{04}	0.23	0.06 ± 0.02

[a]Cross sections are separately normalized for each $k'_a = 0$ and 1 manifold.

Despite the fact that no strong propensity rules are present, we actually observe a slight propensity rule in favor of transitions with odd Δk_a and Δk_c which is seen for *p*-NH_2 in collision with both *p*-H_2 and *o*-H_2, while for collisions of *o*-NH_2 with both *p*-H_2 and *o*-H_2 we notice a more marked propensity in favor of even Δk_a and Δk_c. Furthermore, a propensity rule in favor of transitions with $\Delta k_c = 0$ exists for collisions of both *o*- and *p*-NH_2 with both *o*- and *p*-H_2. This propensity is pointed out in Figs. 9 and 10 where the transitions 4_{13}-3_{13} of *o*-NH_2 and 4_{23}-3_{03} *p*-NH_2 are indeed found to be favored. This trend may be explained by the difficulty of reorienting the angular momentum vector with respect to the axis of the greatest moment of inertia.

Because of the similarity of molecular geometries of H_2O and NH_2, it is interesting to compare the propensity properties of the two systems. From the propensity rules found for the H_2O–H_2 system[47] ($\Delta N_1 = 0, \pm1$; $\Delta k_a = 0, \pm1$; $\Delta k_c = 0, \pm1$), it can be seen that transitions with conservation of k_c or small variation of k_c are also favored for this system, which might be general to C_{2v} molecules.

Finally, as collisions with helium are often used to model collisions with *p*-$H_2(j_2 = 0)$, it is interesting to compare our theoretical results with the experimental state resolved cross sections for rotationally inelastic collisions of $NH_2(^2B_1)$ with He measured by Dagdigian.[18] Dagdigian used a crossed beam experiment and resolved fluorescence spectroscopy to study rotational energy transfer within the NH_2 electronic state. Table I presents close-coupling calculation for NH_2 with *p*-$H_2(j_2 = 0)$ collisions at the kinetic energy 467 cm^{-1} used in experiment. By comparing our results with the experimental relative cross sections out of the $NH_2(N_{1k_ak_c} = 0_{00})$ state induced by collision with He,[18] we found that the *p*-H_2 collisional partner is much more efficient than He for inducing $\Delta N_1 > 1$ transitions. This probably mainly reflects the difference in the interaction potential where the NH_2–H_2 well depth is expected to be much larger than the NH_2–He one. Then we confirm again that for hydrides molecules, He cannot be used as a model for H_2, as already found for HCl[42] or H_2O.[46]

IV. CONCLUSION

We have presented in this paper a study of the interaction between NH_2 and hydrogen molecules. Cross sections for the rotational (de)excitation of *o*- and *p*-NH_2 colliding with both *p*-$H_2(j_2 = 0)$ and *o*-$H_2(j_2 = 1)$ have been computed. All transitions among both the 15 lowest levels of *o*-NH_2 and *p*-NH_2 were considered.

The cross sections for collisions with *para*- and *ortho*-H_2 differ, the magnitude of the *ortho*-H_2 ones being dominant. Propensity rules are discussed and it is found that no rigorous selection rules are defined although transitions with $\Delta k_c = 0$ seem to be slightly favored.

The present results should therefore be adopted in any radiative transfer model of NH_2 in environments with T ≤ 150 K. In particular, Persson *et al.*[2] used a non-LTE radiative transfer model using rate coefficients estimated from an assumed quenching rate coefficient of 5×10^{-11} $cm^3\ s^{-1}$ and radiative selection rules, i.e., $\Delta N_1 = 0, \pm1$; $\Delta k_a = \pm1, \pm3$, etc.; $\Delta k_c = \pm1, \pm3$, etc. Our results indicate that inelastic cross sections corresponding to radiatively forbidden transitions (e.g., $\Delta k_c = 0$) can be as probable as (or even stronger than) those corresponding to radiatively allowed transitions. Hence, previously published NH_2 abundance should be revised accordingly, using our new data.

ACKNOWLEDGMENTS

This work has been supported by the Agence Nationale de la Recherche (ANR-HYDRIDES) Contract No. ANR-12-BS05-0011-01 and by the program "Physique et Chimie du Milieu Interstellaire" (PCMI) funded by CNRS and CNES. We thank the CPER Haute-Normandie/CNRT/s, Electronique, Matériaux. H.G. acknowledges the financial support of the United States Department of Energy (Grant No. DE-SC0015997) and J.L. acknowledges the National Natural Science Foundation of China (Grant No. 21573027).

[1]E. F. van Dishoeck, D. J. Jansen, P. Schilke, and T. G. Phillips, Astrophys. J. **416**, L83 (1993).
[2]C. M. Persson, A. O. H. Olofsson, R. Le Gal, E. S. Wirström, G. E. Hassel, E. Herbst, M. Olberg, A. Faure, P. Hily-Blant, J. H. Black, M. Gerin, D. Lis, and F. Wyrowski, Astron. Astrophys. **586**, A128 (2016); e-print arXiv:1511.05486.
[3]J. R. Goicoechea, N. J. Rodríguez-Fernández, and J. Cernicharo, Astrophys. J. **600**, 214 (2004).
[4]E. T. Polehampton, J.-P. Baluteau, B. M. Swinyard, J. R. Goicoechea, J. M. Brown, G. J. White, J. Cernicharo, and T. W. Grundy, Mon. Not. R. Astron. Soc. **377**, 1122 (2007).
[5]G. Pilbratt, J. Riedinger, T. Passvogel, G. Crone, D. Doyle, U. Gageur, A. Heras, C. Jewell, L. Metcalfe, S. Ott *et al.*, Astron. Astrophys. **518**, L1 (2010).
[6]T. De Graauw, F. Helmich, T. Phillips, J. Stutzki, E. Caux, N. Whyborn, P. Dieleman, P. Roelfsema, H. Aarts, R. Assendorp *et al.*, Astron. Astrophys. **518**, L6 (2010).
[7]P. Hily-Blant, S. Maret, A. Bacmann, S. Bottinelli, B. Parise, E. Caux, A. Faure, E. A. Bergin, G. A. Blake, A. Castets, C. Ceccarelli, J. Cernicharo, A. Coutens, N. Crimier, K. Demyk, C. Dominik, M. Gerin, P. Hennebelle, T. Henning, C. Kahane, A. Klotz, G. Melnick, L. Pagani, P. Schilke, C. Vastel, V. Wakelam, A. Walters, A. Baudry, T. Bell, M. Benedettini, A. Boogert, S. Cabrit, P. Caselli, C. Codella, C. Comito, P. Encrenaz, E. Falgarone, A. Fuente, P. F. Goldsmith, F. Helmich, E. Herbst, T. Jacq, M. Kama, W. Langer, B. Lefloch, D. Lis, S. Lord, A. Lorenzani, D. Neufeld, B. Nisini, S. Pacheco, T. Phillips, M. Salez, P. Saraceno, K. Schuster, X. Tielens, F. van der Tak, M. H. D. van der Wiel, S. Viti, F. Wyrowski, and H. Yorke, Astron. Astrophys. **521**, L52 (2010); e-print arXiv:1009.1119.
[8]C. M. Persson, J. H. Black, J. Cernicharo, J. R. Goicoechea, G. E. Hassel, E. Herbst, M. Gerin, M. de Luca, T. A. Bell, A. Coutens, E. Falgarone, P. F. Goldsmith, H. Gupta, M. Kaźmierczak, D. C. Lis, B. Mookerjea, D. A. Neufeld, J. Pearson, T. G. Phillips, P. Sonnentrucker, J. Stutzki, C. Vastel, S. Yu, F. Boulanger, E. Dartois, P. Encrenaz, T. R. Geballe, T. Giesen, B. Godard, C. Gry, P. Hennebelle, P. Hily-Blant, C. Joblin, R. Kołos,

J. Krełowski, J. Martín-Pintado, K. Menten, R. Monje, M. Perault, R. Plume, M. Salez, S. Schlemmer, M. Schmidt, D. Teyssier, I. Péron, P. Cais, P. Gaufre, A. Cros, L. Ravera, P. Morris, S. Lord, and P. Planesas, Astron. Astrophys. **521**, L45 (2010); e-print arXiv:1007.2550.
[9]R. Le Gal, P. Hily-Blant, A. Faure, G. Pineau des Forêts, C. Rist, and S. Maret, Astron. Astrophys. **562**, A83 (2014); e-print arXiv:1311.5313 [astro-ph.SR].
[10]C. M. Persson, M. De Luca, B. Mookerjea, A. Olofsson, J. H. Black, M. Gerin, E. Herbst, T. Bell, A. Coutens, B. Godard *et al.*, Astron. Astrophys. **543**, A145 (2012).
[11]A. Faure, P. Hily-Blant, R. Le Gal, C. Rist, and G. Pineau des Forêts, Astrophys. J. **770**, L2 (2013).
[12]R. Le Gal, E. Herbst, C. Xie, A. Li, and H. Guo, Astron. Astrophys. **596**, A35 (2016); e-print arXiv:1609.02485.
[13]N. Troscompt, A. Faure, L. Wiesenfeld, C. Ceccarelli, and P. Valiron, Astron. Astrophys. **493**, 687 (2009).
[14]S. Maret, A. Faure, E. Scifoni, and L. Wiesenfeld, Mon. Not. R. Astron. Soc. **399**, 425 (2009).
[15]D. Rabli and D. R. Flower, Mon. Not. R. Astron. Soc. **406**, 95 (2010).
[16]F. Daniel, M.-L. Dubernet, and A. Grosjean, Astron. Astrophys. **536**, A76 (2011).
[17]C. Balança, A. Spielfiedel, and N. Feautrier, Mon. Not. R. Astron. Soc. **460**, 3766 (2016).
[18]P. J. Dagdigian, J. Chem. Phys. **90**, 2617 (1989).
[19]R. N. Dixon and D. Field, Proc. R. Soc. A **366**, 247 (1979).
[20]Y. Kalugina, J. Kłos, and F. Lique, J. Chem. Phys. **139**, 074301 (2013).
[21]A. Faure and F. Lique, Mon. Not. R. Astron. Soc. **425**, 740 (2012).
[22]M. Lanza and F. Lique, J. Chem. Phys. **141**, 164321 (2014).
[23]J. Li and H. Guo, Phys. Chem. Chem. Phys. **16**, 6753 (2014).
[24]M. Yang and J. C. Corchado, J. Chem. Phys. **127**, 184308 (2007).
[25]F. Lique and A. Faure, J. Chem. Phys. **136**, 031101 (2012).
[26]F. Lique, J. Chem. Phys. **142**, 241102 (2015).
[27]B. Jiang, J. Li, and H. Guo, Int. Rev. Phys. Chem. **35**, 479 (2016).
[28]P. B. Davies, D. K. Russell, B. A. Thrush, and H. E. Radford, Proc. R. Soc. A **353**, 299 (1977).
[29]P. Valiron, M. Wernli, A. Faure, L. Wiesenfeld, C. Rist, S. Kedžuch, and J. Noga, J. Chem. Phys. **129**, 134306 (2008).
[30]Y. Scribano, A. Faure, and L. Wiesenfeld, J. Chem. Phys. **133**, 231105 (2010).
[31]A. Faure, P. Jankowski, T. Stoecklin, and K. Szalewicz, Sci. Rep. **6**, 28449 (2016).
[32]J. B. Burkholder, C. J. Howard, and A. R. W. McKellar, J. Mol. Spectrosc. **127**, 415 (1988).
[33]T. R. Phillips, S. Maluendes, A. D. McLean, and S. Green, J. Chem. Phys. **101**, 5824 (1994).
[34]C. Rist and A. Faure, J. Math. Chem. **50**, 588 (2012).
[35]H. S. Müller, H. Klein, S. P. Belov, G. Winnewisser, I. Morino, K. M. Yamada, and S. Saito, J. Mol. Spectrosc. **195**, 177 (1999).
[36]T. R. Phillips, S. Maluendes, and S. Green, J. Chem. Phys. **102**, 6024 (1995).
[37]J. M. Hutson and S. Green, MOLSCAT computer code, version 14, distributed by Collaborative Computational Project No. 6 of the Engineering and Physical Sciences Research Council (UK), 1994.
[38]M. H. Alexander and D. E. Manolopoulos, J. Chem. Phys. **86**, 2044 (1987).
[39]A. Faure, K. Szalewicz, and L. Wiesenfeld, J. Chem. Phys. **135**, 024301 (2011).
[40]L. Wiesenfeld and A. Faure, Mon. Not. R. Astron. Soc. **432**, 2573 (2013).
[41]F. Dumouchel, J. Kłos, and F. Lique, Phys. Chem. Chem. Phys. **13**, 8204 (2011).
[42]M. Lanza, Y. Kalugina, L. Wiesenfeld, and F. Lique, J. Chem. Phys. **140**, 064316 (2014).
[43]Y. Kalugina, O. D. Alpizar, T. Stoecklin, and F. Lique, Phys. Chem. Chem. Phys. **14**, 16458 (2012).
[44]J. Kłos and F. Lique, Mon. Not. R. Astron. Soc. **390**, 239 (2008).
[45]J. Cernicharo, A. Spielfiedel, C. Balança, F. Dayou, M.-L. Senent, N. Feautrier, A. Faure, L. Cressiot-Vincent, L. Wiesenfeld, and J. Pardo, Astron. Astrophys. **531**, A103 (2011).
[46]M.-L. Dubernet, F. Daniel, A. Grosjean, A. Faure, P. Valiron, M. Wernli, L. Wiesenfeld, C. Rist, J. Noga, and J. Tennyson, Astron. Astrophys. **460**, 323 (2006).
[47]A. Faure, N. Crimier, C. Ceccarelli, P. Valiron, L. Wiesenfeld, and M. Dubernet, Astron. Astrophys. **472**, 1029 (2007).